Lawrence Berkeley National Laboratory

Title
Study of non-fusion products in the Ti 50 + Cf 249 reaction

Permalink
https://escholarship.org/uc/item/3tz40898

Authors
Di Nitto, A
Khuyagbaatar, J
Ackermann, D
et al.

Publication Date
2018-09-01

DOI
10.1016/j.physletb.2018.07.058

Peer reviewed

Study of non-fusion products in the ^{50}Ti + ^{249}Cf reaction

A. Di Nitto [a,b], J. Khuyagbaatar [b,c,*], D. Ackermann [b,1], L.-L. Andersson [c,d], E. Badura [b], M. Block [a,b,c], H. Brand [b], I. Conrad [b], D.M. Cox [d], Ch.E. Düllmann [a,b,c], J. Dvorak [c], K. Eberhardt [a,c], P.A. Ellison [e,f], N.E. Esker [e,f], J. Even [a,c,2], C. Fahlander [g], U. Forsberg [g], J.M. Gates [e], P. Golubev [g], O. Gothe [e,f], K.E. Gregorich [e], W. Hartmann [b], R.D. Herzberg [d], F.P. Heßberger [b,c], J. Hoffmann [b], R. Hollinger [b], A. Hübner [b], E. Jäger [b], B. Kindler [b], S. Klein [a], I. Kojouharov [b], J.V. Kratz [a], J. Krier [b], N. Kurz [b], S. Lahiri [h], B. Lommel [b], M. Maiti [h,3], R. Mändl [b], E. Merchán [b], S. Minami [b], A.K. Mistry [d], C. Mokry [a,c], H. Nitsche [e,f], J.P. Omtvedt [i], G.K. Pang [e], D. Renisch [a], D. Rudolph [g], J. Runke [b], L.G. Sarmiento [j,4], M. Schädel [b,k], H. Schaffner [b], B. Schausten [b], A. Semchenkov [i], J. Steiner [b], P. Thörle-Pospiech [a,c], N. Trautmann [a], A. Türler [l,m], J. Uusitalo [n], D. Ward [g], M. Wegrzecki [o], P. Wieczorek [b], N. Wiehl [a], A. Yakushev [b], V. Yakusheva [c]

[a] *Johannes Gutenberg University Mainz, 55099 Mainz, Germany*
[b] *GSI Helmholtzzentrum für Schwerionenforschung GmbH, 64291 Darmstadt, Germany*
[c] *Helmholtz Institute Mainz, 55099 Mainz, Germany*
[d] *University of Liverpool, Liverpool, L69 7ZE, UK*
[e] *Lawrence Berkeley National Laboratory, Berkeley, CA 94720-8169, USA*
[f] *University of California, Berkeley, CA 94720-1460, USA*
[g] *Lund University, 22100 Lund, Sweden*
[h] *Saha Institute of Nuclear Physics, Kolkata-700064, India*
[i] *University of Oslo, 0315 Oslo, Norway*
[j] *Universidad Nacional de Colombia, Bogotá D.C. 111321, Colombia*
[k] *Japan Atomic Energy Agency, Tokai, Ibaraki 319-1195, Japan*
[l] *University of Bern, 3012 Bern, Switzerland*
[m] *Paul Scherrer Institute, 5232 Villigen, Switzerland*
[n] *University of Jyväskylä, 40014 Jyväskylä, Finland*
[o] *Institute of Electron Technology, 02-668 Warsaw, Poland*

ARTICLE INFO

ABSTRACT

The isotopic distribution of nuclei produced in the ^{50}Ti + ^{249}Cf reaction has been studied at the gas-filled recoil separator TASCA at GSI Darmstadt, which separates ions according to differences in magnetic rigidity. The bombardment was performed at an energy around the Bass barrier and with the TASCA magnetic fields set for collecting fusion-evaporation reaction products. Fifty-three isotopes located "northeast" of ^{208}Pb were identified as recoiling products formed in non-fusion channels of the reaction. These recoils were implanted with energies in two distinct ranges; besides one with higher energy, a significant low-energy contribution was identified. The latter observation was not expected to occur according to kinematics of the known types of reactions, namely quasi-elastic, multi-nucleon transfer, deep-inelastic

collisions or quasifission. The present observations are discussed within the framework of two-body kinematics passing through the formation of a composite system.

0. Introduction

During the last decades, heavy-ion induced reactions were largely exploited for various applications aiming to explore the entire chart of nuclei [1]. Especially, great success has been achieved in the region of superheavy elements (SHE) by discovering elements up to $Z = 118$ (Og) in heavy-ion induced complete fusion reactions with subsequent emission of neutrons (fusion-evaporation) [2].

Complete fusion is the final result of the two colliding nuclei, which form a composite system after they have overcome the Coulomb repulsion [3]. However, the probability for fusion, leading to further fission and/or evaporation of light particles from the compound nucleus, may strongly be reduced due to the breaking of the composite system, often referred also as dinuclear system, and depends on the properties of the reactants [4–10]. This increases the probability of the process complementary to fusion denoted as quasifission (QF) [4]. QF becomes predominant in reactions having a high Coulomb force at the entrance channel, which is typically quantified as the charge product of projectile and target nuclei, $Z_p Z_t$ [11]. Accordingly, the fusion probability is strongly hindered and thus reduces fusion-evaporation cross sections of reactions for the synthesis of SHE, where the heavy ions collide with massive target nuclei [5,7,12]. Therefore, an alternative pathway featuring higher production yields for the synthesis of SHE, thus reducing the sometimes very long experimental duration [13] and allowing the synthesis of more neutron-rich isotopes than are accessible via fusion reactions, has been sought for decades [14,15].

Recent theoretical calculations suggest the production of SHE in multi-nucleon transfer reactions [16] often referred also as deep inelastic transfer or strongly damped collisions [17]. Evidently, a classification of these types of reactions, often based on overlapping experimental observables [4,18], does not always properly reflect the evolution of the nuclear reaction. Similarly, no comprehensive theoretical description of these reactions still exists due to a lack of exhaustive data on the observables despite many experimental efforts [19–22]. Regardless different namings and absence of the comprehensive theory, the common feature of these reactions concerns their outcome products, which are well distinguishable from the ones of elastic-types of scattering and fusion-evaporation reactions.

Pioneering studies on such types of reaction have been performed in the late 1970s by applying chemical separation techniques to gain access to relatively long-lived nuclei ($T_{1/2} \geq 1$ h) [23,24]. Recently, in ^{48}Ca + ^{248}Cm reactions [25,26], new short-lived ($T_{1/2} \approx 1$ ms) neutron-deficient isotopes of heavy elements (^{216}U, ^{219}Np, ^{223}Am, ^{229}Am and ^{233}Bk) have been synthesized at the velocity filter SHIP at GSI Darmstadt. These and other known experimental results [27–29] demonstrate that reactions, whose recoiling products have maximum yields at grazing angles (often $>0°$) and wide angular distributions, can be studied at forward angles around 0°.

To further elucidate the origin of nuclear reaction products emitted at near-zero-degree angles, we employed the gas-filled recoil TransActinide Separator and Chemistry Apparatus (TASCA) [30], which exploits a different principle for ion separation compared to SHIP. Thus, the present results obtained by selecting ions from the ^{50}Ti + ^{249}Cf reaction, based on their magnetic rigidities, complement the data from SHIP for ^{48}Ca + ^{248}Cm, where products

were selected by their velocity. In this letter, we report the study on the identification of various nuclei produced in the ^{50}Ti + ^{249}Cf reaction, and the observation of two components of their recoil energies. The latter result has been obtained for the first time in reactions with deformed actinide targets. Fusion products from such reactions are currently the only way to give access to the island of the stability.

Experimental data were accumulated during a long run aimed to synthesize element $Z = 120$ in the fusion-evaporation reaction [31]. Since, the nuclei identified in this work do not belong to decays of either $Z = 120$ nuclei or fusion-fission products (the nuclei with masses around $A = 150$ and around the line of beta stability, [12]), and thus may originate either from QF or multi-nucleon transfer reactions. Therefore, we prefer to refer them as "non-fusion" rather than "transfer" or "target-like" products [27,28].

1. Experimental setup

The experiment was performed at the gas-filled recoil TASCA [30], GSI Darmstadt. 5 ms-long ^{50}Ti^{12+} beam pulses with a repetition rate of 50 Hz and an energy of 306 MeV were provided by the Universal Linear Accelerator. Four arc-shaped ^{249}Cf$_2$O$_3$ targets with an average thickness of (565 ± 6) μg/cm^2 were prepared by electro-deposition onto (2.2 ± 0.2) μm-thick Ti foils [32]. The targets were mounted on a wheel, which rotates synchronously to the beam pulse structure [33]. The beam energy in the center of the target was estimated as 288 MeV [34] at which the largest fusion-evaporation cross section for synthesis of $Z = 120$ element is expected [31].

In this experiment, TASCA was filled with 0.8 mbar helium and its magnetic settings were adjusted to collect ions with magnetic rigidity, $B\rho = 2.14$ Tm in the center of the focal plane [31]. This value corresponds to the expected $B\rho$ of evaporation residues with $Z = 120$ and mass number $A \approx 295$ [35].

Nuclei emerging from the target first traversed a multiwire proportional counter (MWPC) and were subsequently implanted into two Double Sided silicon Strip Detectors (DSSD's). Each 300 μm-thick DSSD having an area of 72×48 mm^2 resulted into total of 144 vertical (X-axis) and 48 horizontal (Y-axis) strips. Thus, products with magnetic rigidities in the range of $B\rho = 1.97$–2.31 Tm were collected in the DSSD. Two single-sided silicon strip detectors were mounted behind the DSSD, with the same dimensions, and were used to register punching-through charged particles. A Combined ANalog and DIgital (CANDI) acquisition system [36,37] was used to process the signals from all detectors. Signals from the 144 vertical strips were connected to the analog branch, where every signal was duplicated and processed in two dynamical ranges up to 20 MeV and 200 MeV. Signals from the 48 horizontal strips were connected to the digital branch of CANDI where their pulse shapes were stored in 50 μs-long traces. The dynamical range of the digital branch, used to read out the horizontal strips, was limited to 35 MeV in order to optimize the α-particle energy resolution. The energy resolution (FWHM) of individual Y-strips was about 40 keV for 8–9 MeV α particles registered as single events in the traces, and about 110 keV for multiple 8–9 MeV α-particle events stored in a single trace with time differences on the order of 1 μs. For a detailed description of TASCA and its detection systems see [28,30,36,37].
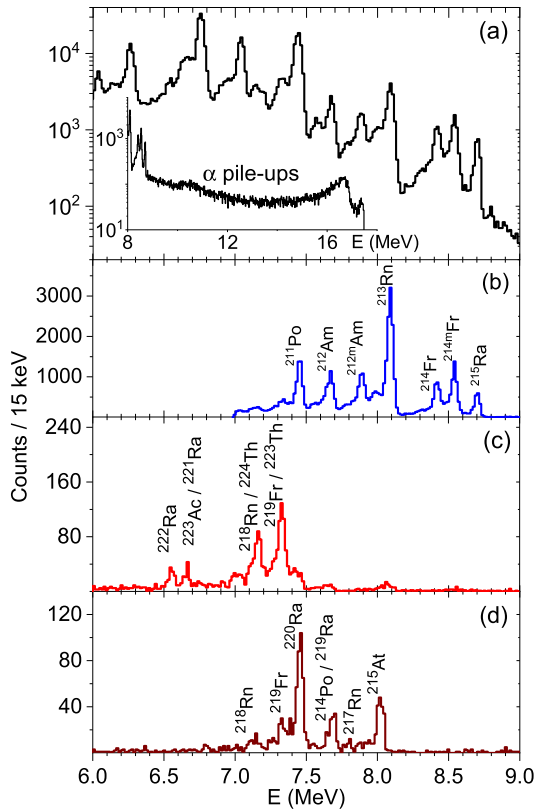
Fig. 1. (Color online.) (a) Energy spectra of beam-off α-like events detected within an energy range of 6–9 MeV without further conditions. The spectrum within an energy range of 8–18 MeV is shown as inset. (b) α particles correlated to their RI signals within 0.5 s. First (c) and second (d) α particles from RI-$\alpha(\leq 100$ s)-$\alpha(\leq 10$ s) correlations.

2. Experimental results

An energy spectrum measured with the DSSD during beam-off periods at an accumulated beam dose of about 4.5×10^{18} part is shown in Fig. 1(a). Energies were extracted from the traces collected with the digital branches (48 Y-strips), by adopting the single-signal amplitude estimation procedure. Several peaks, originating from α decays, are evident on the relatively enhanced background, whose origin is due to the summing of the 48 different Y-strips data and the presence of various pile-up events. The latter correspond to the detection of subsequent α particles within short times ($\lesssim \mu$s), whose energies are summed up and become more evident in the higher energy range, $E = 8$–18 MeV (shown as inset in Fig. 1(a)). Corresponding traces of these multi-signal events were stored and energies extracted with multi-signal amplitude estimation procedure. Therefore, each α-like event, i.e., occurring during beam-off with $E < 18$ MeV, was considered as originating from the decay of an implanted nucleus. We note that in this experiment thousands of fission-like events (DSSD signals with $E > 100$ MeV and in anti-coincidence with MWPC) were detected. However, it was not possible to identify their isotopic origin. Identifications of α lines and pile-ups were achieved in the spatial (X and Y axes) and time correlation analyses, between implantation signals and/or α-like events, and using literature data [38].

According to known properties of non-fusion reactions [26,28], the energies of recoil implantations (RI) were selected to be within the range $E_{RI} = 30$–110 MeV. The RI-like events were required to occur in coincidence with MWPC signals and during beam-on periods.

The first step was the identification of implanted nuclei in RI-α correlations with a search time up to ≤ 0.5 s due to the counting rate for RI-like events. An energy spectrum of such correlated α particles, with $E = 6$–9 MeV is shown in Fig. 1(b). Comparing our experimentally determined half-lives and α energies with literature data, ^{215}Ra, ^{214,214m}Fr, ^{213}Rn, ^{212,212m}At, and ^{211}Po were identified.

Furthermore, RI-α-α, RI-α(7–18 MeV)-α, RI-α(7–18 MeV), RI(pile-up)-α (a note on this correlation will be given below), α-α and α-α-α correlation analyses were performed to identify the remaining peaks and the pile-ups (cf. Figs. 1(a) and (b)). Correlation search times between the members have been varied depending on the correlation types. In α-α-α correlations, for instance, isotopes with $T_{1/2}$ in the order of minutes were possible to be identified. In Figs. 1(c) and 1(d), energy spectra of the first and second α members of RI-α-α correlations are shown as example of the above mentioned analyses. The identification procedure was completed with the analysis of traces stored in the digital branch of CANDI to resolve the pile-up events [36,37]. As a result of this part of the analysis, 37 isotopes were identified as being directly implanted and 11 as daughter or granddaughter of RI's.

In total, 53 isotopes with mass numbers $210 \leq A \leq 226$ and atomic numbers $83 \leq Z \leq 90$ were identified; 42 of them were directly implanted.

Finally, the numbers of events corresponding to peaks at 8.70, 8.48, 8.43, 8.09 MeV in the beam-off spectrum were compared with the deduced numbers of ^{215}Ra, ^{214m}Fr, ^{214}Fr, ^{213}Rn from the correlation analysis (cf. Fig. 1 (a) and (b)) to ensure the statistical agreement. Only 85% of the events were found to be correlated with RI. The remaining 15%, then, were searched in the correlations (e.g., RI-α) where the E_{RI} range was expanded to lower energies.

Energy spectra of RI correlated with α decays of ^{213}Rn, ^{215}Ra and ^{223}Th are shown in Fig. 2(a). Two well separated components are visible for all cases. The RI with energies ≤ 30 MeV account well for those missing 15% mentioned above. The high-energy component (HEC), with $E_{RI} > 30$ MeV, features a peak-like distribution centered at around 70 MeV, while the low-energy component (LEC) has a tail-like shape. Accordingly, part of the LEC may be not detected due to the thresholds of the detection system. Time distributions of RI-α(^{215}Ra) correlations for HEC and LEC events are shown in Fig. 2(b). Both distributions, showing the same half-life of ^{215}Ra, indicate the proper assignment of low energetic recoils.

The LEC recoils could possibly be generated by HEC ones passing through thicker layers (due to inhomogeneities) of the target, MWPC-windows or dead-layers of the DSSD. The spectrum of the ^{249}Cf-α-particles passing through TASCA and the MWPC as measured with the DSSD shows a single well-defined peak. Therefore, significant inhomogeneities of the target, MWPC-windows or dead-layers of the DSSD are negligible. Consequently, we exclude that the LEC can be artificially generated by HEC passing through thicker layers.

The possibility that LEC recoils originate from the scattering of HEC recoils is excluded. The amount of such scattered HEC recoils is negligible taking into account the numbers of observed HEC and the cross sections for the elastic scattering. Therefore, the LEC are most likely associated with the reaction itself. This conclusion is supported from the observed energy losses of LEC and HEC recoils in the MWPC (ΔE) shown in Fig. 2(c). It has been found that the HEC and LEC recoils have lost different amounts of energies in the MWPC, as shown in the case of ^{215}Ra. Such behavior well agrees with the simulated energy losses of recoils with two different kinetic energies shown in Fig. 2(d). Details on simulations are discussed later.
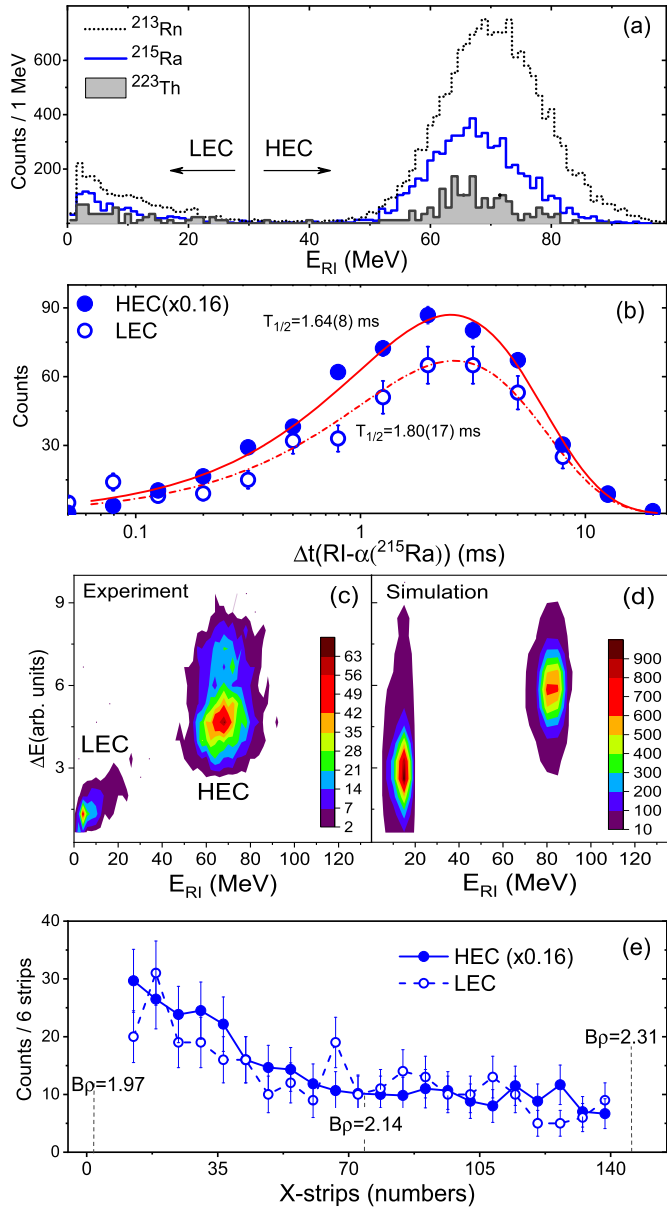
Fig. 2. (Color online.) (a) Implantation-energy distributions of ^{215}Ra, ^{213}Rn, and ^{223}Th isotopes. (b) Time distributions of $\alpha(^{215}$Ra) events in beam-off periods correlated with HEC (multiplied by a factor 0.16) and LEC recoils. The half-lives obtained by fitting experimental data (circles) with universal radioactive decay functions (lines) are consistent with the literature value ($T_{1/2}$=1.67(1) ms [38]). (c) Estimated experimental and (d) SRIM simulated energy losses in the MWPC (ΔE) and DSSD (E_{RI}) detectors of RI of ^{215}Ra events. (e) Relative yields of same events as function of DSSD X-strip of HEC and LEC recoils.

Furthermore, thanks to the small amplitude of RI signals of the LEC events, RI and α signals occurring in a short time (down to a fraction of μs) were recorded with full shapes in single traces within the dynamical range of the used digital electronics system, [39]. Therefore, by analyzing the RI(LEC) traces with multiple signals we could identify the decays of short-lived ^{219}Th, ^{218}Ac, ^{217}Ra, ^{216}Fr and ^{215}Rn nuclei for the first time in this type of experiment.

The distributions of HEC and LEC recoils along the X-strips of the DSSD are shown in Fig. 2(e). The rates of both HEC and LEC recoils increased on the low-Bρ side. Evidently, such distributions point towards a partial collection of recoils with widely spread and much lower average Bρ ($<$1.97 Tm) than the set value (2.14 Tm). The average Bρ of HEC and LEC recoils of ^{215}Ra can be estimated if

their kinetic energies (E_K) and mean charge states are known. We deduced the E_K from the energy measured in the DSSD by taking into account pulse height defects [40] and energy losses [34]. Then, the HEC-peak at 70 MeV corresponds to 150 MeV, and 10 MeV, taken as a representative value for the LEC, correspond to 45 MeV. Considering the E_K of 150 and 45 MeV for HEC and LEC recoils, respectively, and the mean charge states according to the formulas in Ref. [41], we calculated the corresponding Bρ = 1.76 Tm and 1.67 Tm. For the simulations of the Fig. 2(d), we used the above values for kinetic energies.

Therefore, the main part of recoils with such values of Bρ will miss the DSSD, which is in agreement with the observed HEC and LEC distributions (see Fig. 2(e)) and with the above discussion.

The absolute cross sections for the identified nuclei cannot be given due to the unknown efficiencies for their transmission through TASCA and the efficiency for the DSSD coverage (see Fig. 2(e)). To still arrive at a rough value, we take a detection efficiency for full-energy α particles in the DSSD as 55%, and a beam intensity of 3×10^{12} part/s. Under these assumptions, the implantation rates of ^{213}Rn HEC and ^{223}Th LEC, representatives of identified nuclei with high and low rates in the DSSD, respectively, were estimated as 8.1×10^{-3} and 1.3×10^{-4} events per second. These values would correspond to the product of efficiency and cross section ($\sigma\varepsilon$, where ε is the overall efficiency similar to Ref. [26]) of 4.4 and 0.07 nb, respectively. The latter value is our lower $\sigma\varepsilon$ limit for the nuclei identified in the present experiment.

3. Discussion and summary

All fifty-three identified isotopes are located "north-east" of ^{208}Pb, on the N vs. Z plane as shown in Fig. 3(a). The population of nuclei in this region, far from the target, is similar to known experimental findings for reactions with actinide targets measured over a wide angular range [18]. Only data obtained at SHIP for the ^{48}Ca + ^{248}Cm reaction [26] can be compared with the present results. In both works the implanted nuclei have been identified via their characteristic radioactive decay properties. At SHIP, the separation of heavy ions with particular mass and charge state is performed according to ion velocity. In contrast, the separation in TASCA is based on the average magnetic rigidity, where no particularly selected mass, velocity and charge state of ions can be isolated. Moreover, the gas-filled separators often have short lengths (for example 3.5 m of TASCA and 12 m of SHIP) compared to those operating in the vacuum mode thus potentially result to the higher transmission and the short flight path for the products, see Ref. [42]. Studies at both types of separators, potentially completed by radiochemical studies [20], appear best suited to shed further light on the reaction mechanism leading to the formation of these products.

In Fig. 3(a) the isotopic distribution of the ^{48}Ca + ^{248}Cm reaction products is shown together with the present results. Both distributions overlap widely, despite some deviations, such as relatively narrow distribution of isotopes along the N and Z axes in the present data. A comparison of directly implanted nuclei is shown in Fig. 3(b). In the present data the gap between N = 127 and 130, a region containing predominately very short-lived nuclei (mostly decaying during the flight through TASCA), is significantly reduced compared to the ^{48}Ca + ^{248}Cm data, likely thanks to the implementation of a multi-pixelized DSSD and CANDI, as well as to the shorter flight time, about a factor 3, between the target and the implantation detector at TASCA compared to SHIP. It is worth noting that nuclei around/above the ^{249}Cf-target were not identified due to the limited sensitivity of the correlation technique used here.
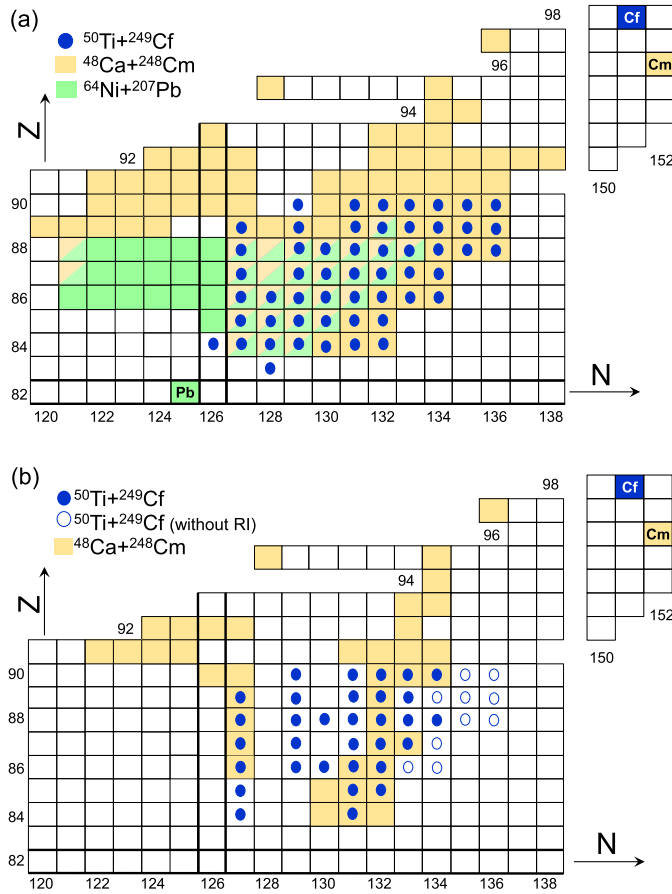
Fig. 3. (Color online.) Cut out of the chart of nuclei in the relevant region [38]. (a) The isotopes identified by their α decay and genetic correlations in ^{50}Ti + ^{249}Cf reactions (blue circles) are compared with those identified in ^{64}Ni + ^{207}Pb [43] and ^{48}Ca + ^{248}Cm [26] reactions marked in green and orange, respectively. (b) Isotopes directly implanted into the focal plane detector. The filled (empty) blue circles correspond to ^{50}Ti + ^{249}Cf reaction products identified in correlation analyses with (without) RI-like events. The orange frames relate to ^{48}Ca + ^{248}Cm reaction products observed in correlation with RI-like events [26,25].

The isotopic distribution of the ^{50}Ti + ^{249}Cf reaction products can be affected if the target comprised a Pb contamination, which can also produce similar products in ^{50}Ti + Pb reactions. However, this contribution is likely negligible taking into account the upper limit of lead impurity ($<<1\%$) and the expected N–Z distributions of reactions with Pb, cf. the data for the ^{64}Ni + ^{207}Pb reaction included in Fig. 3(a) [27].

One can also compare the $\sigma\varepsilon$ values of directly implanted nuclei in the ^{50}Ti + ^{249}Cf and ^{48}Ca + ^{248}Cm reactions [26]. For quantitative aspects of this discussion it is important to bear in mind that the TASCA settings were set to maximize the efficiency for fusion products, whereas SHIP was operated at settings better suited for non-fusion products. In Fig. 4 the $\sigma\varepsilon$ values for Th, Ac and Ra isotopes are shown as function of N. In general, a similar behavior of the present data to those of the ^{48}Ca + ^{248}Cm reaction [26] can be noticed most pronounced for Th isotopes despite the differences in terms of reactions and separation techniques. Nevertheless, deviations in the absolute values exist and can be attributed to factors including the different overall efficiencies of the two separators and reactions. For instance about 4 times lower values, on average for Th isotopes, obtained at TASCA may be due to the partial collection by the DSSD of recoils reaching the focal plane of TASCA (see Fig. 2(e)) and/or to the differences in the population of them through nucleon exchange process. By assuming that the $\sigma\varepsilon$ for
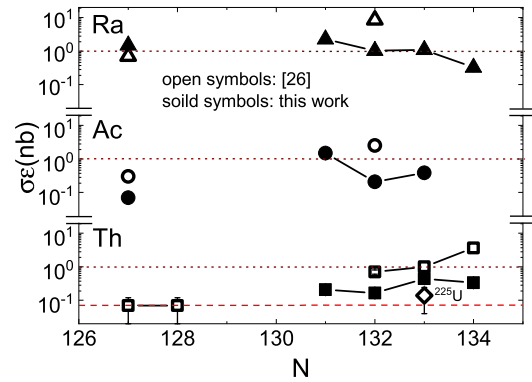

Fig. 4. (Color online.) Product of cross section and efficiency, $\sigma\varepsilon$, for directly implanted Th, Ac and Ra isotopes. The ^{50}Ti + ^{249}Cf reaction values (solid symbols) are compared with the ^{48}Ca + ^{248}Cm reaction ones (open symbols) [26]. The ^{225}U $\sigma\varepsilon$ (open diamond) from [26] was also included in the lower panel as representative of products with $Z > 90$. The dashed lines show the 1 nb level and the dotted line the $\sigma\varepsilon$ lower limit for the non-fusion products identification in the present experiment.

U isotopes is on average reduced by a factor 4 compared to SHIP ones [26], similarly to the Th case, one can expect to detect ^{225}U at TASCA with a $\sigma\varepsilon$ of 0.03 nb. This value is below the experimental sensitivity for non-fusion products in this work, thus this latter can be the reason for the non-observation of ^{225}U. Instead, the non-observation of other U isotopes cannot be explained by the lower cross section limit argument, having been measured with cross sections significantly higher than ^{225}U at SHIP. However, we avoid to provide an interpretation on the $\sigma\varepsilon$ of heavier U isotopes, not included in Fig. 4, because they were extracted in an analysis that did not include RI-like events.

The nuclei observed in the ^{50}Ti + ^{249}Cf and ^{48}Ca + ^{248}Cm reactions originate from a process where a large number of nucleons flows in the direction of the projectile nucleus with cross sections significantly higher than the fusion-evaporation ones. Significant mass exchange from target to projectile often indicates nuclear reactions occurring on reaction timescales that are long enough to allow the formation of a dinuclear system, but short enough for it to break before complete mass equilibration is achieved, i.e., favoring QF and/or multi-nucleon transfer, which are known to produce the observed nuclei.

The above arguments are supported by the known features of fusion systematics. According to this, a strong hindrance for fusion in the ^{50}Ti + ^{249}Cf fusion is expected [12]. This follows from the criteria of the charge numbers of projectile and target products, where the present reaction has $Z_p Z_t = 2156$, which is far above the lower limit (≈ 1600), beyond which the fast QF process is known to set in, according to Ref. [11].

It is well known that the heavy fragments from QF of heavy-ion induced reactions with actinide targets reveal mass distributions with maxima around $A = 215$–220 [12,5,7,8], due to the influence of the doubly magic ^{208}Pb. Thus, nuclei observed in this work – and also in ^{48}Ca + ^{248}Cm – could originate from QF.

The observed two components in implantation energies of nuclei from the ^{50}Ti + ^{249}Cf reaction, thus, could be explained with dynamical properties of the QF process. Since QF typically occurs during the rotation of the dinuclear system, the heavy fragment with mass A emitted with a velocity v_{cm} at different angles in the center of mass frame θ_{cm} can be detected in the laboratory frame within wide angular and velocity ranges. According to Ref. [27], the two energy components of heavy fragments can be explained by emission of them at $\theta_{cm} = 0°$ and $180°$, i.e. along the beam axis, with velocities of $v_{HEC} = v_{cm} + v_{CN}$ and $v_{LEC} = v_{cm} - v_{CN}$, respectively, where v_{CN} is the velocity of the compound nucleus in the laboratory frame. However, if $v_{CN} > v_{cm}$ the heavy fragments

Table 1

Experimental and calculated kinetic energies, E_K, (in MeV) and emission directions (forward ($\rightarrow$) or backward ($\leftarrow$) in the laboratory frame) of heavy fragments (RI) from the three reactions. Two cases of their emissions in the center of mass frame ($\theta_{cm} = 0°$ and $\theta_{cm} = 180°$ corresponding to HEC and LEC, respectively) are given for three reactions, whose beam energies (E_{lab} in MeV) are indicated. The isotope ^{215}Ra was considered in the first reaction, ^{215}Ra and ^{223}Th for the second, and ^{226}Ac for the third. All experimental data were measured in the forward direction in the laboratory system.

Reaction	E_{lab}	RI	HEC ($\theta_{cm} = 0°$) E_K (Dir.)		LEC ($\theta_{cm} = 180°$) E_K (Dir.)	
			Exp.	Calc.	Exp.	Calc.
^{64}Ni ^{207}Pb	360	^{215}Ra	194[a] ($\rightarrow$)	193 ($\rightarrow$)	10[a] ($\rightarrow$)	8.5 ($\rightarrow$)
^{50}Ti + ^{249}Cf	288	^{215}Ra	150 ($\rightarrow$)	182 ($\rightarrow$)	45* ($\rightarrow$)	2.9 ($\leftarrow$)
		^{223}Th	142 ($\rightarrow$)	176 ($\rightarrow$)	44* ($\rightarrow$)	1.7 ($\leftarrow$)
^{48}Ca + ^{248}Cm	256	^{226}Ac	110[b] ($\rightarrow$)	151 ($\rightarrow$)	–	1.2 ($\leftarrow$)

[a] Deduced from measured velocities in Ref. [27].
[b] Deduced from measured velocities in Ref. [26].
* Representative value for the LEC.

emitted at $\theta_{cm} = 180°$ would not be detected at backward angles, but instead in forward direction in the laboratory frame as in the case of $\theta_{cm} = 0°$. In such cases, heavy fragments with two different velocities will be observed at forward angles, similar to the present findings showing a HEC and a LEC. Only one such experimental case is known for the ^{64}Ni + ^{207}Pb reaction [27], where two velocity components for non-fusion products (shown in Fig. 3) have been measured. Measured velocities for both components have been calculated within the above mentioned approach, where v_{cm} was deduced from the TKE according to the Viola systematics for QF with an asymmetric mass split [44]. A fair agreement between the estimated and experimental velocities was reached, supporting the suggested scenario for the explanation of the HEC and LEC [27]. Therefore, within this approach, an interpretation of the present data can be given. Moreover, we calculated the energies of the LEC and HEC of these identified products, namely ^{215}Ra and ^{223}Th. To gain insight on this approach we have given in Table 1 the velocities of the LEC and HEC, expressed in terms of E_K, and emission directions in the laboratory frame resulting from calculations together with the experimentally deduced ones.

The results for ^{215}Ra from the ^{64}Ni + ^{207}Pb reaction are also shown in Table 1, where both HEC and LEC have been detected in the forward direction.

At first, we calculate the energies for ^{215}Ra for which both HEC and LEC have been observed in the ^{64}Ni + ^{207}Pb and ^{50}Ti + ^{249}Cf reactions. In the case of the LEC, the calculated v_{cm} was larger than the v_{CN} (cf. Table 1) for the ^{50}Ti + ^{249}Cf reaction, which means that ^{215}Ra is emitted in backward directions, i.e. no detection of the LEC in forward direction is expected. Similarly, the calculated LEC velocity of the heavier isotope ^{223}Th also prevents this from entering into the TASCA acceptance angle. At the same time, experimental E_K of HEC are overestimated in both cases, ^{215}Ra and ^{223}Th. Therefore, the present results have poor numerical agreements with the calculations in both the HEC and the LEC. These deviations could be due to non-directly measured experimental energies of ^{215}Ra and ^{223}Th, for which only rough estimates for both HEC and LEC are given. However, the velocity of HEC of ^{226}Ac from the ^{48}Ca + ^{248}Cm reaction have directly been measured at the velocity filter SHIP, thus, one can compare it with the calculation. Despite the measurement technique for the HEC-energy, ^{226}Ac is still overestimated by a similar amount ($\approx$25–35%) as in the case of the present data, cf. Table 1. Accordingly, deviations could be associated with the overestimation of the QF TKE and/or due to the kinetic-energy dissipation in the heavy fragment. Observation of the LEC of ^{226}Ac in ^{48}Ca + ^{248}Cm reactions is not predicted by the calculations, as one could expect. We note that due to the lack of experimental data, this cannot presently be confirmed.

It could be inferred that a quantitative description of the kinetic energies of non-fusion products from the ^{50}Ti + ^{249}Cf and ^{48}Ca + ^{248}Cm reactions cannot be given within the current knowledge on the TKE of the QF. However, a qualitative explanation via the QF scenario is still possible. This, though, would substantially profit from further dedicated experiments on the kinematics of non-fusion products from ^{50}Ti + ^{249}Cf and/or similar reactions.

Finally, in this letter we demonstrated that the forward-angle gas-filled separator can be used for the study of the non-fusion reaction mechanisms and, consequently, TASCA can be suitable for the synthesis of the exotic nuclei originating in other reaction channels than fusion-evaporation. The observations at TASCA reported here provide a stimulus for future explorations with optimized operation of gas-filled separators for the isolation of non-fusion products to tap the full potential of this method for the investigation of nuclei with low-production yield. Fifty-three isotopes of elements from Bi to Th, identified with help of the advanced detection system, shows the sudden disappearance of the detection yield of the elements $Z > 90$ in the non-fusion reaction channels that is somehow different from the results obtained at the velocity filter SHIP. Presently, we cannot draw a final conclusion on the reason for deviations in the isotopical distributions, because different experimental techniques, detection setups and reactions were adopted in the two experiments. Therefore to disentangle the influence of the different aspects responsible of such deviations, it appears ideal to investigate the same target/projectile combination at different types of separators, like SHIP and TASCA, under identical reaction conditions. Nevertheless, we note that production yields of U isotopes suddenly decreases compared to those of Th ones according to the fusion-evaporation reaction data. For instance, in the ^{48}Ca + ^{176}Yb reaction Th isotopes are produced with cross section values in the order of 100 µb [45], whereas the cross sections of U isotopes in the ^{50}Ti + ^{176}Yb reaction are only few nb [37]. Furthermore to define the limits of the isotopical distributions, one should consider the measurements of β-decaying and/or long-lived nuclei for which different detection techniques are required compared to those presently employed. Recently, such a setup which includes the combination of the chemical separation and high efficient measurements of ALpha, BEta and GAmma decays ALBEGA is under final construction [46]. The most intriguing result of the present work is the observation of recoils emitted at forward angle with energy distribution showing two components which seem to be associated with reaction mechanism of the particular non-fusion channel. By considering the significant nucleon flow populating the nuclei located "north-east" of ^{208}Pb and the observation of two energy components, the possible origin of the identified isotopes was suggested to be quasifission for which forward-angle data scarcely exist. The results of the present work motivate further studies on nuclear reactions aimed at examining the presence of a low-energy component and providing wide-range isotopic distributions that could shed light on the understanding of the different reaction mechanisms.

Environmental Health and Safety Division for their support with the preparation and execution of the ^{249}Cf shipment to Germany.

References

[1] B.B. Back, et al., Rev. Mod. Phys. 86 (2014) 317.
[2] Yu.Ts. Oganessian, V.K. Utyonkov, Rep. Prog. Phys. 78 (2015) 036301.
[3] R. Bass, Nuclear Reactions with Heavy Ions, Springer-Verlag, Berlin, 1980.
[4] J. Töke, et al., Nucl. Phys. A 440 (1985) 327.
[5] E.M. Kozulin, et al., Phys. Lett. B 686 (2010) 227.
[6] M.G. Itkis, et al., Phys. Rev. C 83 (2011) 064613.
[7] K. Nishio, et al., Phys. Rev. C 86 (2012) 034608.
[8] D.J. Hinde, et al., EPJ Web Conf. 131 (2016) 04004.
[9] J. Khuyagbaatar, et al., Phys. Rev. C 91 (2015) 054608.
[10] J. Khuyagbaatar, et al., Phys. Rev. C 97 (2018) 064618.
[11] W.J. Swiatecki, Phys. Scr. 24 (1981) 113.
[12] M.G. Itkis, et al., Nucl. Phys. A 944 (2015) 204.
[13] Yu.Ts. Oganessian, J. Phys. G 34 (2008) R165.
[14] J.V. Kratz, et al., Phys. Rev. C 33 (1986) 504.
[15] Yu.Ts. Oganessian, A. Sobiczewski, G.M. Ter-Akopian, Phys. Scr. 92 (2017) 023003.
[16] V.I. Zagrebaev, W. Greiner, Phys. Rev. C 83 (2011) 044618.
[17] V.V. Volkov, Phys. Rep. 44 (1978) 93.
[18] H. Gäggeler, et al., Phys. Rev. C 33 (1986) 1983.
[19] L. Corradi, G. Pollarolo, S. Szilner, J. Phys. G 36 (2009) 113101.
[20] J.V. Kratz, W. Loveland, K.J. Moody, Nucl. Phys. A 944 (2015) 117.
[21] M. Schädel, EPJ Web Conf. 131 (2016) 04001.
[22] M. Götz, et al., Nucl. Phys. A 961 (2017) 1.
[23] M. Schädel, et al., Phys. Rev. Lett. 41 (1978) 469.
[24] M. Schädel, et al., Phys. Rev. Lett. 48 (1982) 852.
[25] H.M. Devaraja, et al., Phys. Lett. B 748 (2015) 199.
[26] S. Heinz, et al., Eur. Phys. J. A 52 (2016) 278.
[27] S. Heinz, et al., Eur. Phys. J. A 51 (2015) 140.
[28] J. Gates, et al., Phys. Rev. C 83 (2011) 054618.
[29] J. Konki, et al., Phys. Lett. B 764 (2017) 265.
[30] A. Semchenkov, et al., Nucl. Instrum. Methods B 266 (2008) 4153.
[31] Ch.E. Düllmann, et al., to be published.
[32] J. Runke, et al., J. Radioanal. Nucl. Chem. 299 (2014) 1081.
[33] E. Jäger, et al., J. Radioanal. Nucl. Chem. 299 (2014) 1073.
[34] J.F. Ziegler, M. Ziegler, J. Biersack, in: 19th International Conference on Ion Beam Analysis, Nucl. Instrum. Methods B 268 (2010) 1818.
[35] J. Khuyagbaatar, et al., Phys. Rev. A 88 (2013) 042703.
[36] J. Khuyagbaatar, et al., Phys. Rev. Lett. 112 (2014) 172501.
[37] J. Khuyagbaatar, et al., Phys. Rev. Lett. 115 (2015) 242502.
[38] G. Audi, et al., Chin. Phys. C 41 (2017) 030001.
[39] J. Khuyagbaatar, et al., EPJ Web Conf. 131 (2016) 03003.
[40] B. Wilkins, et al., Nucl. Instrum. Methods 92 (1971) 381.
[41] K.E. Gregorich, et al., Phys. Rev. C 72 (2005) 014605.
[42] M. Leino, Nucl. Instrum. Methods B 126 (1997) 320.
[43] V.F. Comas, et al., Eur. Phys. J. A 112 (2013) 49.
[44] M. Wilpert, et al., Phys. Rev. C 51 (1995) 680.
[45] C.C. Sahm, et al., Nucl. Phys. A 441 (1985) 316.
[46] A. Di Nitto, et al., GSI Scientific Report 2014, 2015, p. 184.